Blinded Evaluation of Planar Technetium-99m-Sestamibi Myocardial Perfusion Studies

Denny D. Watson, William H. Smith, George A. Beller, Ellen L. Vinson, and Raymond Taillefer

Division of Medical Imaging, Department of Radiology, and Division of Cardiology, Department of Internal Medicine, at the University of Virginia Health Sciences Center, Charlottesville, Virginia and Department of Nuclear Medicine, Hotel-Dieu de Montreal, Montreal, Canada

Sestamibi planar myocardial perfusion studies were performed at Hotel-Dieu de Montreal on 28 patients with documented coronary artery disease and 16 normal subjects. Stress and rest studies were performed on separate days. These studies were sent to Virginia for interpretation while blinded as to age, sex, and other clinical information. Studies were quantitated independently by two operators (using a computer program modified for Sestamibi), and interpreted independently by two experienced interpreters. Computer quantitation of 2816 segments gave an average interoperator deviation of 2.2%. Pure quantitative criteria were applied for computer interpretation. By varying the detection threshold, we produced the entire ROC curve relating sensitivity and specificity as a function of detection threshold. Using only computer criteria for normal or abnormal, interoperator agreement by patient was 98% and 93% by view. The computer could achieve equal positive and negative predictive accuracy of 87%. Interpreters, allowed both quantitative and subjective judgment, agreed on 91% of 44 patients, 90% of 132 views, and 92% of 660 segments. Interpreters averaged 94% positive and 86% negative predictive accuracy.

J Nucl Med 1992; 33:668–675

New ^{99m}Tc-labeled myocardial perfusion agents have been long awaited and are now released for clinical use in the United States. Clinical trials of sestamibi (Cardiolite®—DuPont, N. Billerica, MA), a ^{99m}Tc-labeled isonitrile, have been conducted and early experience appears promising for its utility to detect coronary artery disease (CAD) and delineate myocardial infarction. Some results of multicenter clinical trials of this agent have been published (*1,2*). Other investigations have indicated the myocardial extraction and kinetic transport of sestamibi (*3–6*); the potential use of this agent for differentiation of viable from infarcted myocardium (*7–10*); the use of ECG gating with sestamibi (*11,12*); and preliminary experience for detection of CAD (*13,14*).

Received Jul. 30, 1991; revision accepted Dec. 13, 1991.
For reprints contact: Denny D. Watson, Nuclear Cardiology, Box 468-65, University of Virginia Health Sciences Center, Charlottesville, VA 22908.

This paper reports the results of an entirely blind reading of 44 planar sestamibi studies performed at Hotel Dieu de Montreal and mailed to the University of Virginia for computer quantitation and interpretation. Quantitative computer processing was performed using a program designed specifically for sestamibi (*15*). The interpreters were completely unaware of any clinical or demographic data that could indicate pretest likelihood of disease and therefore potentially bias scan readings.

The purpose of this study was to determine how well interpreters experienced in ^{201}Tl imaging could read sestamibi studies with the aid of quantitative image processing in terms of inter-interpreter agreement, agreement with coronary angiographic findings and ^{201}Tl perfusion studies. Studies were also analyzed according to purely quantitative criteria. This allowed us to generate receiver operating characteristic (ROC) curves of sensitivity and specificity, as a function of threshold for defect detection.

MATERIALS AND METHODS

Patient Population

The study cohort comprised 15 volunteers and 29 patients with suspected CAD and abnormal perfusion by ^{201}Tl exercise scintigraphy. The volunteers had <5% likelihood of CAD based on Bayesian analysis of age, sex, symptom classification, and normal exercise ^{201}Tl scintigraphy. Catheterization was not performed on the volunteers. Of the 29 patients with suspected CAD, one had angiographically normal coronary arteries and 28 had significant CAD defined as >70% luminal diameter narrowing of one or more coronary arteries. Of these, 15 had a clinical history of prior myocardial infarction. The patient with angiographically normal coronary arteries was added to the normal volunteer group, yielding 16 subjects in the normal group. All studies were performed at the Hotel-Dieu d'Montreal in Quebec. The information on the composition of the patient population was completely unknown to the interpreters of the sestamibi images at the University of Virginia.

Stress and Rest Sestamibi Imaging Protocol

Two separate injections were used to perform the sestamibi studies with 1–3 days between injections. For stress images, patients followed the Bruce protocol and were injected intravenously with 20–25 mCi of sestamibi at peak exercise followed by 1 min of additional exercise. Imaging commenced 60–90 min after injection in the 45° left anterior oblique (LAO) projection,

followed sequentially by anterior and 70° LAO projections. Following a resting injection of 20–25 mCi, imaging began 75–100 min later using the same imaging sequence. All sestamibi images were recorded for a preset time of 10 min, using a 64 × 64 matrix size in a 20% window centered on the 140-keV gamma ray peak of ^{99m}Tc. Images were acquired on a Medical Data System (MDS) computer.

Quantitative Image Analysis

Images were mailed on diskettes to the University of Virginia for quantitative analysis and visual interpretation. The University of Virginia investigators were given only the patient code and were blinded to all other data, including the patient's sex or the percentage of normals in the population. A quantitative program originally developed for ^{201}Tl (*16*) was modified for sestamibi imaging as previously described (*15*). Important features of the original program include display normalization and calibration, minimal operator dependence, background subtraction, and image registration. The following modifications were made for use with sestamibi:

1. The interpolative background subtraction algorithm was modified because of the difference in heart-to-background ratio and shape of the extracardiac background between resting and exercise sestamibi images (*15–20*).
2. With sestamibi, suboptimal display of the heart is caused by excessive ^{99m}Tc activity in the viscera. The program automatically suppresses extracardiac activity if it exceeds the maximum activity in the heart (*15*).
3. Since two separate injections are necessary in sestamibi imaging, the rest and exercise profiles must be scaled differently. Exercise profiles are displayed with the maximum value at full scale. The resting profiles are then displayed so the maximum value of the resting profiles will be at 75% of full scale. Stress and rest profiles can then be overlapped for comparison without the two curves being on top of each other. The overlapped curves are ideally scaled to show regions of reversibility.

All patient studies were independently quantitated by two experienced operators on a Sophy P 32-bit microcomputer (Sopha Medical—Columbia, MD). The resulting images and count profiles were independently interpreted by two experienced readers.

Image Display and Interpretation

The reproducibility of image interpretation depends on a standardized method of image display. Since image interpretation was to be performed by reading from video monitors, we used the test pattern developed by the Society of Motion Picture and Television Engineers (SMPTE) (*21*) to set the video contrast and brightness levels. We also used a standardized intensity scale that we designed (*15,22*) to relate image count density linearly to perceived brightness.

The computer program saves the quantitated results on disk for later recall using a special display program designed for ease of interaction with the interpreter. Figure 1 illustrates the different display formats that are available to the interpreters. Figure 1A and 1B are the standard formats for exercise and rest images. Four count profiles (each ≈1 cm wide) span the heart. In Figure 1B, the exercise and rest profiles are overlapped for better comparison.

Another feature used by the interpreters is the "flashback display" (*15*). This display capability is useful for the detection of subtle defect reversibility. The background-corrected images are brought into alignment using image registration techniques previously described (*15,16,23*) and each scaled to its maximum count. With a single keystroke the interpreter can cause the exercise image to appear in the position occupied by the rest image. The shift between images is extremely swift and smooth, and since the images are precisely aligned, there is no apparent motion of the myocardium. If a defect is reversible, that myocardial segment will have increased relative uptake of sestamibi, which will appear as a sudden shift in the intensity of the ischemic region when the flashback is employed. The flashback display exploits the eye's superb ability to detect sudden changes in an otherwise static image, thus enabling an intuitive and sensitive method of visually identifying reversibility.

Two expert ^{201}Tl interpreters at the University of Virginia (DDW, GAB) independently read the quantitated sestamibi images from video monitors using the display program described above. The readers were blinded to age, sex, other clinical information and the prevalence of CAD in this population. Each interpreter was isolated and readings were recorded on a form that was signed and mailed before the clinical data was sent to Virginia from Montreal. Fifteen segments were graded by the two interpreters, five per view. Each view was divided into five equal segments with the apex in the middle and two segments to each side of the apex. Each segment was graded as either normal (NL), persistent defect (PD), or reversible defect (RD). A view was automatically graded as RD if any segment showed reversibility. If a view showed a defect with no reversible segments, then the view was graded as PD. If the view had only normal segments, then it was graded as NL. Patients were automatically graded in a similar fashion. Also, a patient or view was determined to be abnormal if the resulting grade was PD or RD.

Automatic Computer Measurements

Peak activity for selected myocardial segments was automatically measured by the computer along four count profiles for each view (*18*). Each profile was divided into two segments at the vertical centroid line through the heart yielding eight segments per view. Profiles through the valve planes were excluded, yielding 16 segments for analysis. There were five segments in the anterior view, including proximal anterolateral, distal anterolateral, apical, inferior and inferobasilar; five segments in the 70° LAO view, including proximal and distal anterior, apical, inferior and posterior; and six segments in the 45° LAO view, including upper and midseptum, inferoseptal, inferolateral, mid and upper posterolateral. The peak activity for a given segment was found by searching from centroid to edge for the maximum value (in the background-corrected image). The segmental activity values were then normalized by dividing each segment in a particular view by the average of the highest five percentile of profile values in the corresponding view. This is done by first sorting the numerical values from all myocardial samples into descending order and averaging the top five percentile. This avoids normalizing to the single highest value, which would be normalizing to the most extreme statistical outlier from a large number of samples. Normalized values greater than 100% were set to 100%. The normalized values were then converted to defect percentages by subtracting from 100%.

Interoperator variability was measured by computing the root

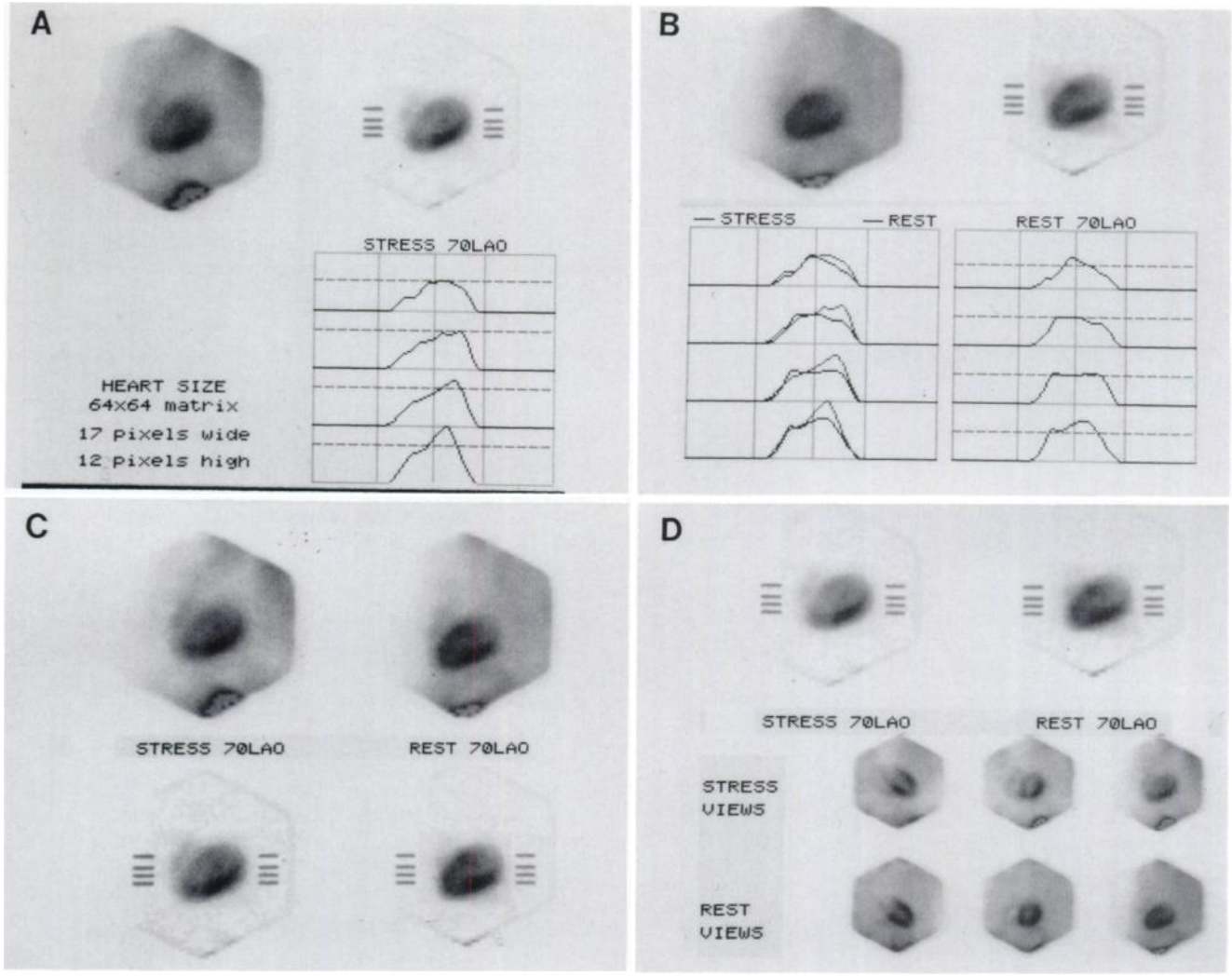

FIGURE 1. (A) The standard display for exercise images is shown. The raw image is displayed (automatically rescaled if necessary) in the upper left quadrant. The background-corrected image is shown in the upper right. Four count profiles (each ~1 cm wide) span the heart and are displayed in the lower right quadrant. (B) The standard display for rest images is similar to that of the exercise images. In addition, in the lower left quadrant the exercise and rest profiles are overlapped for better comparison (remember that the rest profiles have been automatically scaled to 75% of the exercise profiles). (C) Side-by-side image display shows the stress-rest pair of raw images above with the corresponding background-corrected images below. (D) Survey display shows all six raw images below with a user-selectable stress-rest background-corrected pair above.

mean square (RMS) deviation of the defect percentage from the mean of the operators over the entire set of 2816 segments.

To investigate computer operator variability, the following quantitative criteria were established for computer interpretation. A significant initial defect was defined as >25% for all exercise segments except >30% for the inferior sample of the anterior view, the upper septal sample of the 45° LAO view, and the posterior sample of the 70° LAO view; and >40% for the infero-basilar sample of the anterior view. These thresholds are the same as our thallium standards (*16*) but with the upper septal sample adjusted to compensate for slightly greater base-to-apex gradient typical of sestamibi (*18,19*).

Reversibility was arbitrarily defined as a significant initial defect, within any of the 16 sample regions, that improved at least 10 percentage points in the same sample region in the rest study. Using the above criteria, the computer automatically graded each myocardial segment as either NL, PD, or RD. Views and patients were then automatically graded as described in the previous section.

Statistical and ROC Analysis

The results of the expert and computer interpretations were mailed to Montreal to signify completion of the image analysis phase. The blind was then broken and the composition of the patient population and the catheterization results were sent by facsimile to Virginia for final statistical analysis.

The mean and standard deviation was computed for each myocardial segment in the patients identified as normal. These values are shown in Figure 2 for stress studies (solid line) and rest studies (dashed line). The normal values for rest and stress studies were nearly identical ($r = 0.97$) and were averaged together. This result indicates that the background subtraction (*17–19*) had correctly compensated for the different extracardiac background found in the rest studies compared to stress. The Z-score for each

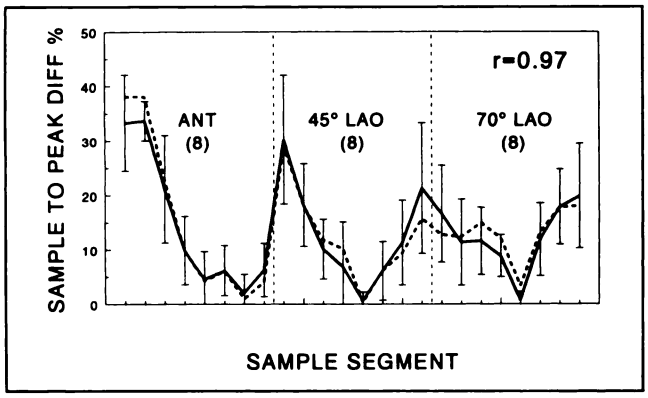

FIGURE 2. Shows the percentage difference comparing sample segment to average peak activity for all 24 segments sampled by the computer in the normal population. The solid line is for stress studies and the dashed line for rest studies. There is no significant difference, indicating that the background subtraction has correctly compensated for differences in extracardiac uptake.

segment was then computed using the average and standard deviation obtained from the normal data base. For every subject, the average of the highest and next highest segment Z-score was obtained. Averaging the two highest defect scores is done to reduce statistical variation that would result from selecting the single most deviant sample from many samples. The Z-score indicates the number of standard deviations each patient varies from the normal average based on the two most deviant segments. We then set thresholds that varied from 0.5 to 10 standard deviations. For each threshold, a patient was classified as abnormal if the exercise study varied from the normal average by more than the threshold deviation. For each different threshold, the false-positive rate and true-positive rate was determined. This data is plotted to create the ROC curve. For low thresholds, the sensitivity is high but the specificity is low. For high thresholds, the specificity is high but the sensitivity is low. The ROC analysis indicates the tradeoff between sensitivity and specificity.

RESULTS

Observer Interpretation

Table 1 is a summary of the expert and computer interpretations broken down by patient. As shown in Table 2, for Observer 1, the predictive accuracy of a positive test was 96% (24/25) and the predictive accuracy of a negative test was 79% (15/19). Observer 2 had corresponding predictive accuracies of 93% (27/29) and 93% (14/15). Table 2 also shows the predictive accuracy obtained after excluding all patients with history of prior myocardial infarction. Table 3 indicates the characteristics of the patient population. In Table 4, the agreement between the expert interpreters is broken down by category. The interpreters agreed at least 90% of the time on patient, view, and segment. The concordance by segment is shown in Figure 3. Interpreters disagreed most often on apical segments. Disagreement was greater on the judgment of redistribution than on classification of normal versus abnormal.

TABLE 1
Patient Summary of Expert and Computer Interpretations

Patient code	Previous infarct	Computer #1	Computer #2	Observer #1	Observer #2	Group
ALLRE	No	NL	NL	NL	NL	NL
BACNO	Yes	RD	RD	RD	RD	CAD
BAYGI	Yes	RD	RD	RD	RD	CAD
BEAFE	No	RD	RD	RD	RD	CAD
BELLO	No	NL	NL	NL	NL	NL
BOICL	No	NL	NL	NL	NL	NL
BROAN	No	NL	NL	RD*	RD*	NL
CHACL	Yes	PD	PD	PD‡	RD	CAD
CHAJO	No	RD	RD	RD	RD	CAD
CHEAN	No	NL	NL	NL	NL	NL
CLOCA	Yes	PD	PD	RD‡	PD	CAD
DAOBE	Yes	RD	RD	RD	RD	CAD
DUBGI	No	NL	PD*	NL†	NL	NL
DUPJE	Yes	RD	RD	RD	RD	CAD
GIGJE	No	NL*	NL*	NL*	NL*	CAD
HAMMA	No	NL*	NL*	RD	RD	CAD
HEBGI	No	NL	NL	NL	NL	NL
JEAAL	No	NL	NL	NL	NL	NL
JOLRO	Yes	RD†	PD	RD	RD	CAD
LADYV	No	NL	NL	NL	NL	NL
LAMRA	No	NL	NL	NL	NL	NL
LANRI	No	RD	RD	RD	RD	CAD
LARSE	No	NL	NL	NL	NL	NL
LAUYV	Yes	RD	RD	RD	RD	CAD
LECCH	No	RD*†	PD*	NL	NL	NL
LEMFR	No	NL	NL	NL	NL	NL
LERAL	No	RD	RD	RD	RD	CAD
LOPHU	Yes	RD	RD	RD	RD	CAD
MAHHA	Yes	NL*	NL*	RD	RD	CAD
MALAN	No	RD	RD	RD	RD	CAD
MALJA	Yes	PD	PD	RD	RD	CAD
MONPI	Yes	RD	RD	RD	RD	CAD
OUEMA	No	NL*	NL*	RD	RD	CAD
PARFR	No	NL*	NL*	NL*‡	RD	CAD
POIHE	No	NL	NL	NL	NL	NL
QUEMI	Yes	NL*	NL*	NL*‡	RD	CAD
RICRO	Yes	PD	PD	RD	RD	CAD
RICYV	No	PD	PD	RD	RD	CAD
ROYDA	No	RD	RD	RD	RD	CAD
ROYEG	No	NL*	NL*	NL*‡	RD	CAD
STHAN	Yes	RD	RD	RD	RD	CAD
TAIRA	No	NL	NL	NL‡	RD*	NL
TETGA	No	RD	RD	RD	RD	CAD
VILDA	No	NL	NL	NL	NL	NL

* Denotes disagreement with group.
† Denotes disagreement between computer operators.
‡ Denotes disagreement between expert interpreters.

TABLE 2
Predictive Accuracy of Observers

	Predictive accuracy	Observer #1	Observer #2
All patients	Positive	0.96	0.93
	Negative	0.79	0.93
Excluding	Positive	0.91	0.86
Prior MI	Negative	0.83	0.93

TABLE 3
Patient Characteristics

	Normal group (n = 16)	CAD group (n = 28)
Age (yr)	41.1 ± 7.3	53.9 ± 8.6
Sex (% male)	88%	79%
Previous MI	0	15 (54%)
Peak heart rate (bpm)	165.5 ± 11.7	132.9 ± 16.8
Peak systolic BP (mmHg)	146.7 ± 17.5	143.3 ± 22.9

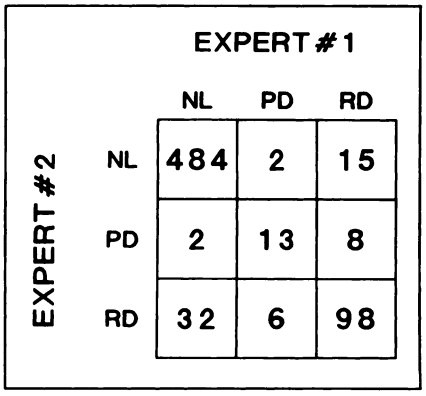

FIGURE 3. Illustrates the concordance between the expert interpreters for the 660 segments graded in the study. The exact agreement was 90.2% (595/660).

Computer Interpretation

The patient summary of the computer interpretations is shown in Table 1. The two different operators obtained different computer classification of normal versus abnormal on only one patient. In only two patients did the two computer operators disagree with respect to PD versus RD. Table 5 tabulates the agreement between operators by category. The agreements were uniformly high. The interoperator RMS deviation for 2816 segments averaged 2.2%.

Thresholds for Defect Detection

Figure 4 shows the sensitivity for defect detection as a function of the threshold level set to detect a defect. This curve is derived from the subset of patients with CAD. Also shown in Figure 4 is the specificity or false-positive rate as a function of the threshold for defect detection. This curve shows a rapid loss of specificity since the threshold is reduced below about two standard deviations from the normal population. The sensitivity curve shows a gradual falloff of sensitivity since the threshold for defect detection is increased. This graph does not extend to show all the defects. The largest defects in the CAD population ranged to over 40 standard deviations. This shows a wide deviation of defects in patients with CAD ranging from extremely abnormal to where there are no defects statistically distinguishable from the normal population. Figure 5A includes all the data used to produce a conventional ROC curve. This curve shows how sensitivity and specificity vary by using different thresholds for detection of CAD. Also plotted on this graph is the sensitivity and specificity combination obtained from the two interpreters. The interpreters scored somewhat higher than the computer alone, presumably by exercising judgment that was not programmed into the computer. Figure 5B is the ROC curve and interpreter scores obtained after excluding all patients with history of prior myocardial infarction.

TABLE 4
Interpreter Agreement

Category	By patient	By view	By segment: Exact match	By segment: NL/AB match
Total	40/44	119/132	595/660	609/660
	91%	90%	90%	92%
Normals	15/16	47/48	238/240	238/240
	94%	98%	99%	99%
Abnormals	25/28	72/84	357/420	371/420
	89%	86%	85%	88%
Anterior	—	41/44	199/220	205/220
		93%	90%	93%
45° LAO	—	42/44	195/220	200/220
		95%	89%	91%
70° LAO	—	36/44	201/220	204/220
		82%	91%	93%

Each column shows the agreement divided by the total possible with the percent agreement shown below. The interpreters were scored on their determination of whether a patient (or view) was normal (NL) or abnormal (PD, RD). In the exact match by segment column, both interpreters had to give a segment the same grade, either NL, PD, or RD, for an exact agreement. In the NL/AB match by segment column, the interpreters had only to concur that a segment was normal (NL) or abnormal (PD, RD) for agreement.

TABLE 5
Computer Agreement

Category	By patient	By view	By segment: Exact match	By segment: NL/AB match
Total	43/44	123/132	681/704	690/704
	98%	93%	97%	98%
Normals	15/16	46/48	253/256	254/256
	94%	96%	99%	99%
Abnormals	28/28	77/84	428/448	436/448
	100%	92%	96%	97%
Anterior	—	40/44	211/220	213/220
		91%	96%	97%
45° LAO	—	41/44	257/264	260/264
		93%	97%	98%
70° LAO	—	42/44	213/220	217/220
		95%	97%	99%

Each column shows the agreement divided by the total possible with the percent agreement shown below. The computer scored the operators on their determination of whether a patient (or view) was normal (NL) or abnormal (PD, RD). In the exact match by segment column, the computer had to give a segment the same grade for each operator, either NL, PD, or RD, for an exact agreement. In the NL/AB match by segment column, the computer had only to concur that a segment was normal (NL) or abnormal (PD, RD) for each operator for agreement.

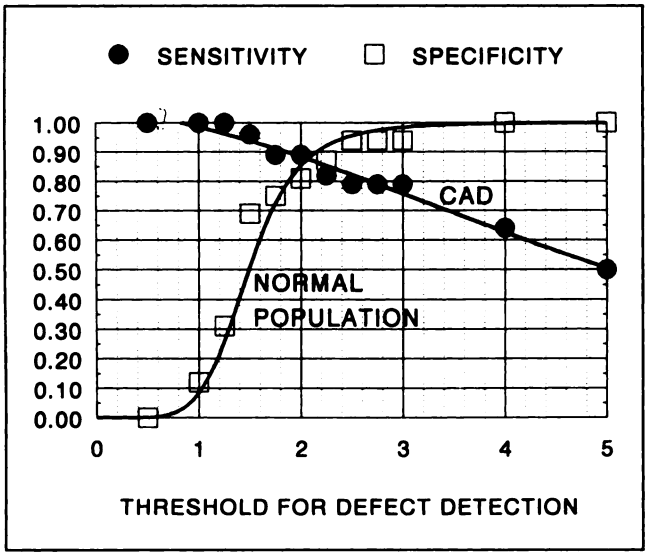

FIGURE 4. Sensitivity and specificity are shown as a function of the threshold (horizontal axis) used to separate normal from abnormal. The values (Z-scores) on the horizontal axis represent the number of standard deviations from normal. The curves show that 10% to 15% of the CAD group were statistically indistinguishable from the normal group and can be identified only at the expense of increasing false positives.

DISCUSSION

This study demonstrates that sensitivity and specificity can both be maintained at reasonably high levels with planar sestamibi imaging. The interpreters were experienced readers of ^{201}Tl but not sestamibi scintigrams. Differences exist between the two radionuclides that required significant modification of the computer program used for quantitative analysis. However, after these modifications were made, little adjustment was required by the interpreters for correct interpretation. The population in this study is clearly biased by the inclusion of normal volunteers and a moderately high incidence of patients with history of prior myocardial infarction. However, a notable feature was the completely blinded interpretation of the sestamibi studies. The data were collected in one institution and sent to a second institution for interpretation. Observers were blinded even to whether a study was of a male or female and had no idea of the percentage of normal and abnormal subjects included in the cohort.

Interpretation entirely based on computer criteria was performed to generate the ROC curves. ROC analysis is essential to properly characterize sensitivity and specificity because it defines the entire range of these variables and defines the tradeoff of specificity for sensitivity. A knowledge of the entire curve is necessary to judge the power of the test to discriminate between normal and abnormal patients.

Figure 4 is an illuminating alternative to the conventional ROC plot. In this figure, the specificity curve is derived from the normal sub-population. This curve indicates that there were few normal subjects with defects more than three standard deviation units away from the normal mean but about 15% of normals that deviated by

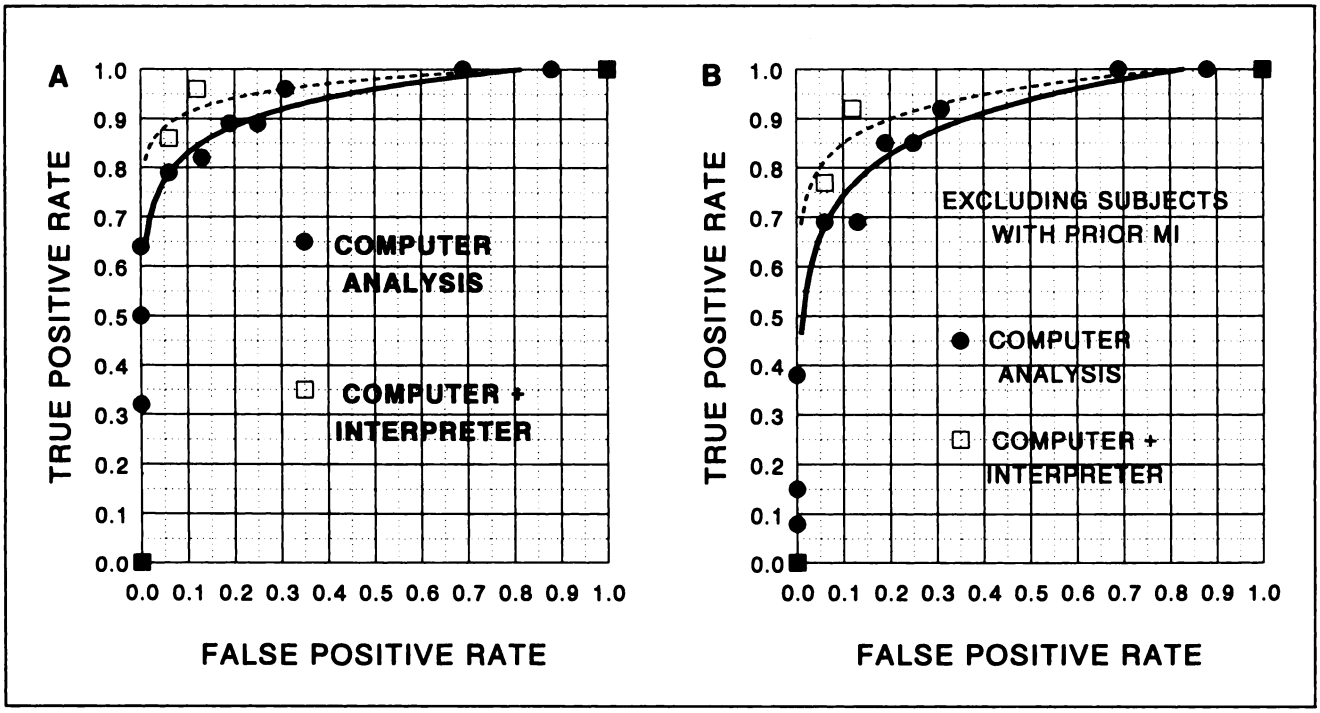

FIGURE 5. (A) Standard ROC curve showing the true-positive rate (specificity) on the vertical axis and the false-positive rate (1-specificity) on the horizontal axis. The solid dots represent computer results at various detection thresholds. The open squares are the result of the interpretation by two experienced observers. (B) ROC curve obtained after excluding all patients with history of myocardial infarction.

two standard deviation units. This is expected, assuming normally distributed deviations from the mean. The curve of sensitivity is obtained from the sub-population with CAD and this group has what might seem to be an unexpected, extremely broad distribution. The most floridly abnormal subjects (not plotted) extended to more than 40 standard deviations away from normal. At the other end of this spectrum, slightly more than 10% of the CAD group had a myocardial uptake pattern that was statistically indistinguishable from the normal population. Thus, we find about 10% of the population with angiographically significant coronary artery abnormalities, who nevertheless do not have a significant maldistribution of sestamibi. While this subgroup of patients has CAD by angiographic criteria, it is reasonable that most of these patients do not have significant maldistribution of myocardial blood flow. In that sense, some of these "false-negatives" may be correct in the sense of indicating homogeneity of myocardial perfusion. The only way to increase the sensitivity so as to "detect" disease in this subgroup is to lower the threshold into the range of normal patients and accept a higher false-positive rate.

Note that we could produce a 95% sensitivity by accepting a 40% false-positive rate. We prefer to maintain a balanced sensitivity and specificity and can achieve an equal sensitivity and specificity of about 85% by purely quantitative criteria or about 90% with expert interpretation added. As discussed above, it would be unrealistic to expect much better separation of normals from patients with hemodynamically significant coronary disease, given that there will be some cases where coronary anatomy does not exactly predict myocardial perfusion. Moreover, our normal population was biased with normal volunteers, which probably produced a normal distribution with less spread than from normal patients referred for evaluation.

Other studies have looked at the sensitivity and specificity of sestamibi for detection of CAD. The clinical efficacy of sestamibi planar stress and rest imaging was assessed in a multicenter Phase II clinical trial involving 38 patients from several institutions (*1*). Of 36 patients with significant CAD, 35 (97%) had abnormal ^{201}Tl stress images and 32 (89%) had abnormal sestamibi images. The slight increase in ^{201}Tl sensitivity (not statistically significant) may be attributed to the fact that most patients in the trial were enrolled based on having an abnormal ^{201}Tl scan on the imaging study performed for clinical indications. Other studies employing planar or SPECT imaging techniques have also demonstrated that exercise and rest sestamibi imaging is comparable to stress-redistribution ^{201}Tl scintigraphy for detection and localization of CAD (*14,24,25*).

A unique feature of the present study is the totally blinded nature of the scintigraphic interpretation employing quantitative image analysis. The generation of ROC curves for sensitivity and specificity as a function of threshold for sestamibi defect detection is also unique to this study.

ACKNOWLEDGMENT

The assistance of DuPont Pharma in converting the data from MDS to Sopha compatible diskettes is gratefully acknowledged.

REFERENCES

1. Wackers FT, Berman DS, Maddahi J, et al. Technetium-99m hexakis-2-methoxyisobutyl isonitrile: human biodistribution, dosimetry, safety and preliminary comparison to thallium-201 for myocardial perfusion imaging. *J Nucl Med* 1989;30:301–311.
2. Taillefer R, Dupras G, Sporn V, et al. Myocardial perfusion imaging with a new radiotracer, technetium-99m-hexamibi (methoxy isobutyl isonitrile): comparison with thallium-201 imaging. *Clin Nucl Med* 1989;14:97–100.
3. Okada RD, Glover D, Gaffney T, Williams S. Myocardial kinetics of technetium-99m-hexakis-2-methoxy-2-methylpropyl-isonitrile. *Circulation* 1988;77:491–498.
4. Li Q, Frank TL, Franceschi D, Wagner HN, Jr., Becker LC. Technetium-99m-methoxyisobutyl isonitrile (RP-30) for quantification of myocardial ischemia and reperfusion in dogs. *J Nucl Med* 1988;29:1539–1548.
5. Leppo JA, Meerdink DJ. Comparison of the myocardial uptake of a technetium-labeled isonitrile analogue and thallium. *Circ Res* 1989;65: 632–639.
6. Sinusas AJ, Watson DD, Cannon JM, Beller GA. Effect of ischemia and postischemic dysfunction on myocardial uptake of technetium-99m-labeled methoxy-isobutyl isonitrile and thallium-201. *J Am Coll Cardiol* 1989;14:1785–1793.
7. Wackers F, Gibbons R, Verani M, et al. Serial quantitative planar Technetium-99m isonitrile imaging in acute myocardial infarction: efficacy for non-invasive assessment of thrombolytic therapy. *J Am Coll Cardiol* 1989; 14:861–873.
8. Gibbons RJ, Verani MS, Behrenbeck T, et al. Feasibility of tomographic technetium-99m hexakis-2-methoxy-2-methylpropyl isonitrile imaging for the assessment of myocardial area at risk and the effect of treatment in acute myocardial infarction. *Circulation* 1989;80:1277–1286.
9. Rocco RP, Dilsizian V, Strauss HW, Boucher CA. Technetium-99m isonitrile myocardial uptake at rest. II. Relation to clinical markers of potential viability. *J Am Coll Cardiol* 1989;14:1678–1684.
10. Tatum JL, Rehr RB, DiSciascio G, Romhilt DW, Fratkin MJ. Thallium-201/technetium-99m-RP-30a disparity in the course of myocardial infarction after attempted reperfusion. *J Nucl Med* 1988;29:1283–1286.
11. Najm YC, Timmis AD, Maisey MN, et al. The evaluation of ventricular function using gated myocardial imaging with Tc-99m-MIBI. *Eur Heart J* 1989;10:142–148.
12. Marcassa C, Marzullo P, Parodi O, Sambuceti G, L'Abbate A. A new method for noninvasive quantitation of segmental myocardial wall thickening using technetium-99m-methoxy-isobutyl-isonitrile scintigraphy—results in normal subjects. *J Nucl Med* 1990;31:173–177.
13. Taillefer R, Lambert R, Dupras G, et al. Clinical comparison between thallium-201 and Tc-99m-methoxy isobutyl isonitrile (hexamibi) myocardial perfusion imaging for detection of coronary artery disease. *Eur J Nucl Med* 1989;15:280–286.
14. Kiat H, Maddahi J, Roy L, et al. Comparison of technetium-99m methoxyisobutylisonitrile and thallium-201 for evaluation of coronary artery disease by planar and tomographic methods. *Am Heart J* 1989;117:1–11.
15. Smith WH, Watson DD. Technical aspects of myocardial planar imaging with Tc-99m sestamibi. *Am J Cardiol* 1990;66:16E–22E.
16. Watson DD, Campbell NP, Read EK, Gibson RS, Teates CD, Beller GA. Spatial and temporal quantitation of planar thallium myocardial images. *J Nucl Med* 1981;22:577–584.
17. Sinusas AJ, Smith WH, Brookeman V, Vinson E, Beller GA, Watson DD. Quantitative imaging with technetium-99m-methoxyisobutyl isonitrile (RP-30): comparison with Tl-201 using a new background subtraction algorithm [Abstract]. *Circulation* 1987;76:217.
18. Sinusas AJ, Beller GA, Smith WH, Vinson EL, Brookeman V, Watson DD. Quantitative planar imaging with technetium-99m-methoxyisobutyl isonitrile: comparison of uptake patterns with thallium-201. *J Nucl Med* 1989;30:1456–1463.
19. Koster K, Wackers FJ, Mattera JA, Fetterman RC. Quantitative analysis of planar technetium-99m-isonitrile myocardial perfusion images using modified background subtraction. *J Nucl Med* 1990;31:1400–1408.
20. Watson DD, Smith WH. Sestamibi and the issue of tissue crosstalk [Editorial]. *J Nucl Med* 1990;31:1409–1411.

21. Gray JE, Lisk KG, Haddick DH, Harshbarger JH, Oosterhof A, Schwenker R, Members of the SMPTE Subcommittee on Recommended Practices for Medical Diagnostic Display Devices. Test pattern for video displays and hard-copy cameras. *Radiology* 1985;154:519–527.
22. Watson DD, Leidholtz E, Beller GA, Teates CD. Defect perception in myocardial perfusion images [Abstract]. *J Nucl Med* 1980;21:P61–P62.
23. Read ME, Watson DD, Read EK, Leidholtz E. A method for automatic overlapping of sequential scintiphoto images [Abstract]. *J Nucl Med* 1980; 21:P61.
24. Kahn JK, McGhie I, Akers MS, et al. Quantitative rotational tomography with ^{201}Tl and ^{99m}Tc-methoxy-isobutyl-isonitrile. A direct comparison in normal individuals and patients with coronary artery disease. *Circulation* 1989;79:1282–1293.
25. Iskandrian AS, Heo J, Kong B, et al. Use of technetium-99m isonitrile (RP-30A) in assessing left ventricular perfusion and function at rest and during exercise in coronary artery disease, and comparison with coronary arteriography and exercise thallium-201 SPECT imaging. *Am J Cardiol* 1989;64:270–275.

(continued from page 5A)

FIRST IMPRESSIONS

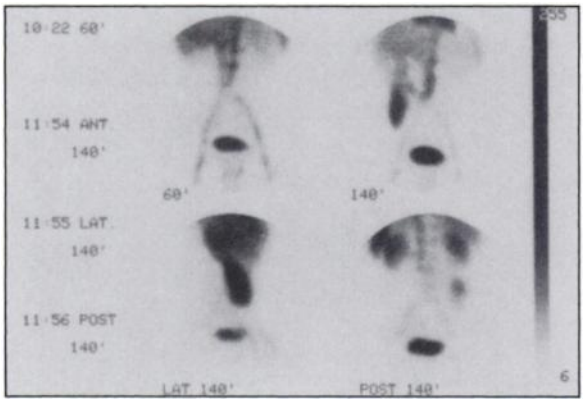

Figure 1

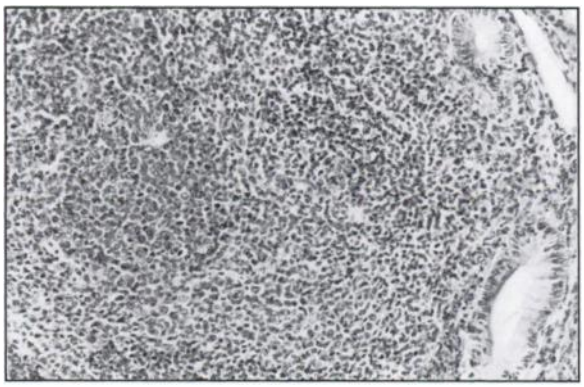

Figure 2

PURPOSE
A 55-yr-old patient with recurrent rectal bleeding was imaged with ^{99m}Tc-red cells. Images were recorded at 5, 10, 15, 30, 60, 140, 180 min and 9 hr after tracer administration (Fig. 1). At 140 min, a well-defined area in the right colon appeared, clearly demonstrating a new episode of bleeding. After surgical exploration, histological data confirmed pseudolymphomatosis (Fig. 2) of the ileum with superficial erosion of the mucosa.

TRACER
^{99m}Tc-RBCs

ROUTE OF ADMINISTRATION
Intravenously

TIME AFTER INJECTION
5, 10, 15, 30, 60, 140, 180 min and 9 hr postinjection

INSTRUMENTATION
Gamma camera (Elscint)

CONTRIBUTORS
Sergio Baldari, MD, Giorgio Restifo, MD and Prof. Nunzio Bonanno, MD

INSTITUTION
Institute of Radiological Sciences, University of Messina, Messina, Italy